Cold Regions Science and Technology 199 (2022) 103569

Contents lists available at ScienceDirect

Cold Regions Science and Technology

journal homepage: www.elsevier.com/locate/coldregions

Topological acoustic sensing of ground stiffness: Presenting a potential means of sensing warming permafrost in a forest

Trevor D. Lata [a,*], Pierre A. Deymier [a], Keith Runge [a], Régis Ferrière [b,c,d], Falk Huettmann [e]

[a] Department of Materials Science and Engineering, University of Arizona, Tucson, AZ 85721, USA
[b] Institut de Biologie de l'ENS, Ecole Normale Supérieure, Université PSL, CNRS, INSERM, 46 rue d'Ulm, 75005 Paris, France
[c] Department of Ecology and Evolutionary Biology, University of Arizona, Tucson, AZ 85721, USA
[d] iGLOBES International Research Laboratory, CNRS, Ecole Normale Supérieure, Université PSL, University of Arizona, Tucson, AZ 85721, USA
[e] EWHALE lab- Institute of Arctic Biology, Biology & Wildlife Department, University of Alaska Fairbanks, Fairbanks, AK 99775, USA

ARTICLE INFO

Keywords:
Geometric phase
Permafrost
Subsurface temperature
Seismic waves
Acoustics

ABSTRACT

The exploitation of sound as a remote sensing platform for environmental monitoring is a novel avenue for detecting changes in subsurface temperatures and properties in permafrost. We present a workflow for using the geometric phase of ground-supported acoustic waves (i.e., seismic waves) due to scattering by trees in a forest as a means of detecting global changes in permafrost stiffness. We work with a simulated environment composed of discrete masses and springs as a testbed for the vibrational response of a forest. For two different spatial distributions of trees, the geometric phase of ground-supported acoustic waves is numerically calculated using MATLAB to show how changes in ground stiffness, due e.g., to changes in subsurface temperature, affect changes in the phase. For acoustic waves with frequencies near the resonant frequencies of the trees the phase is shown to vary more drastically with ground stiffness. This topological acoustic workflow may present a new approach to characterizing changes in permafrost and provide early warning of thawing permafrost, which is vital to maintaining infrastructure and access to natural resources.

1. Introduction

Melting of permafrost in arctic, ocean, and alpine ground drives strong feedbacks of climate warming of the atmosphere, as large amounts of greenhouse gases (CO_2 and methane) are released in the process (Schuur et al., 2015). This makes the detection and mapping of the rate of permafrost thaw a critical component for improving global climate models. Additionally, melting permafrost poses a challenge to local communities in the form of thermokarst formation, changes to ground hydrological properties, and subsidence. These phenomena act to change landscapes for ecosystem services, infrastructure, and access to resources (Ford et al., 2010; Nitze et al., 2018). The foremost threat to infrastructure comes from subsidence, or depression in ground, along transportation lines such as highways, railways (Hjort et al., 2018) and broadband internet lines. There has been considerable attention paid to remote sensing techniques to obtain continuous information on the changing conditions within the arctic. Permafrost can occur in varying degrees of continuity and remains widely unmapped. Boreholes and drilling sites remain the main source of data used to construct rough permafrost maps such as in Fig. 1; this method does not lend itself to continuous monitoring. Current approaches to remote permafrost sensing and mapping rely on directly or indirectly measuring characteristics associated with permafrost regions such as active layer thickness, subsurface ground temperature, the depth to the top of the permafrost layer (National Research Council, 2014), and even the nutrient colour of the vegetation (Döpper et al., 2021). Current remote sensing techniques heavily rely on aerial and satellite imaging that indirectly measure ground characteristics through the reflection of electromagnetic waves (e.g., LiDAR). Such optical methods are limited by their inability to address features of an environment outside of a direct field of view. To bypass the constraints of optical obstructions, acoustics provide an alternate approach for remote sensing. In terrestrial environments, sound carried through the ground, seismic waves, can be used to detect subterranean processes (Trapeznikov and Maleev, 2019; James et al., 2019; Ajo-Franklin et al., 2017). Seismic methods for monitoring the state of permafrost are for the most part based on changes in the velocity of compressional- and/or shear-waves following freezing or thawing of the soil (Hatlelid and MacDonal, 1982; Kneisel

* Corresponding author at: 1235 E. James E. Rogers Way, Tucson, AZ 85721, USA.
E-mail address: tlata157@email.arizona.edu (T.D. Lata).

https://doi.org/10.1016/j.coldregions.2022.103569
Received 26 July 2021; Received in revised form 22 February 2022; Accepted 18 April 2022
Available online 21 April 2022

et al., 2008). The soil velocities directly relate to the elastic properties of the frozen or thawed ground. The velocities increase drastically upon freezing. Here we propose a new method of terrestrial acoustic remote sensing that can detect changes in the ground properties of (densely or sparsely) forested landscapes, such as permafrost thawing in arctic biomes, based on changes in the phase of ground supported acoustic waves. This method is based on the analysis of the effect of trees on the scattering phase of seismic waves, and how this effect changes as the ground properties change.

Traditional acoustic remote sensing platforms rely on frequency responses, spectral analysis, and incidence reflections (De and Chakraborty, 2011; Turk et al., 2011). Such platforms have been used extensively to locate deposits of natural gas and oil with varying degrees of impact on the environment (Kanevskiy et al., 2019; Linke et al., 2005). Topological acoustics has grown to include geometrical factors in the analysis and application of acoustic waves (Deymier and Runge, 2017; Zhang et al., 2018). Traditional methodologies only exploit the frequency (ω) or the wave vector (k) components of acoustic waves, however, topological acoustics expands upon the suite of characteristics available for analysis by involving amplitude (A) and phase (η). Topological acoustics utilizes information encoded in the geometrical amplitude and phase of sound waves arising from symmetry breaking conditions, such as trees scattering the acoustic wave. These geometrical attributes of the wave are sensitive to the interaction of the acoustic wave with its environment, therefore these attributes can be analysed to detect changes in wave-scattering features of an environment.

Anthropic and natural activities are sources of sound that permeate tundra and forested landscapes (Mullet et al., 2016). Seismic waves, acoustic waves carried by the ground, propagate easily in ground and thus provide a rich and widely unexplored opportunity to probe features of the terrain. As seismic waves traverse a forested environment, they are scattered by trees, thus changing the phase of the seismic waves (Colombi et al., 2016). Additionally, the change in phase is influenced by the stiffness of the ground itself. As sub-surface temperatures change in permafrost, the elastic modulus, or stiffness, of the permafrost changes. Thus, the resonances of trees in forested environments can be used to amplify and detect changes in ground stiffness caused by warming permafrost.

2. Methods and models

2.1. Methods

The conventional approach to acoustic sensing has relied on the spectral response of an environment's sound field. The geometric phase of acoustic waves (η) has hitherto been excluded from conventional approaches. There exists an intimate connection between an acoustic wave's η and its Green's function (Deymier and Runge, 2017). The acoustic Green's function is the point response of a system given an impulse stimulus at another point in the system. Due to the point-response nature of the Green's function, it depends on both the position of the response and the position of the stimulus, as well as an eigenvalue, which is effectively the frequency of the acoustic wave squared, $E = \omega^2$.

The Green's function is a complex function, containing both a real and imaginary component. We consider first a normalized Green's function $\widehat{G} = \frac{G}{\sqrt{G^* G}}$ where G^* is the complex conjugate of G. We have $\widehat{G}(E) \propto e^{-i\eta(E)}$. The derivative of $\widehat{G}$ is calculated with respect to the eigenvalue E:

$$\frac{d\widehat{G}(E)}{dE} = \frac{1}{\sqrt{G^* G}} \frac{dG}{dE} - \frac{G}{2(G^* G)^{3/2}} \frac{d(G^* G)}{dE} \tag{1}$$

From (1) it is possible to derive the Berry connection (BC) (Berry, 1984) as a function of the eigenvalue. The Berry connection is given as the following expression:

$$BC(E) = -i\, Tr\left(\widehat{G}^*(E) \frac{d\widehat{G}(E)}{dE}\right) \tag{2}$$

In Eq. (2), Tr is the trace over the entire spatial domain spanned by the Green's function. The Berry connection is associated with changes in the geometric phase of the acoustic wave, η, which is influenced by the whole environment supporting the wave. Eq. 2 can be physically interpreted as the variation in η as a function of the eigenvalue E, or

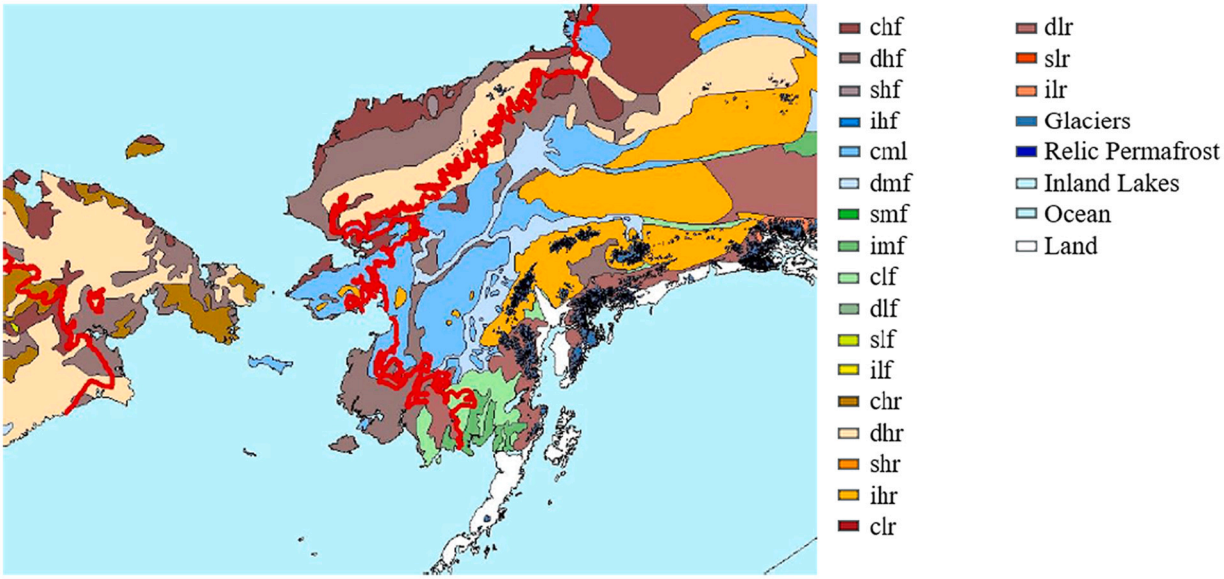

Fig. 1. GIS map of permafrost for the Alaskan region constructed from data provided by the National Snow and Ice Data Centre (Brown et al., 2002). Most regions are classified using a three letter code as follows: first letter denotes permafrost distribution as c- continuous (90–100%), d- discontinuous (50–90%), s- sporadic (10–50%), and i- isolated (0–10%); the second letter denotes ice content as h- high (>20% if followed by an "f", >10% if followed by an "r"), m- medium (10–20%), and l- low (0–10%); the third letter denotes landform type as f- lowlands, highlands, intra- and intermontane depressions with thick top layer (>5–10 m) above permafrost, r- mountains, highland ridges, and plateaus with thin (<5–10 m) top layer above permafrost. The continuous red line denotes the treeline for the region. (For interpretation of the references to colour in this figure legend, the reader is referred to the web version of this article.)

effectively the frequency. This highlights that the change in phase of a wave as it propagates through an environment depends on its frequency – this becomes important when the supporting environment contains resonating scatterers with well-defined characteristics frequencies.

By exploiting some well-studied identities of the Green's function (see Appendix A of Lata et al., 2020, for details), we show that:

$$BC(E) = \frac{d\eta(E)}{d\mathrm{E}} = -Im(TrG) \tag{3}$$

Eq. (3) in essence relates η to the problem of acoustic waves being scattered by an environment. The geometric phase η as a function of frequency can be measured experimentally since it is the phase accumulated by a wave resulting from scattering by its environment. The sensitivity of the geometric phase near the resonant frequencies of these features can be exploited to detect and quantify changes in other properties of the environment, such as changes in ground physical properties.

2.2. Model

We develop a model for calculating the phase, η, of an environment accommodating for tree distribution and ground properties. The materials of the environment are assumed to be linearly elastic. The method is detailed in Appendix A. This simulated model forest is used to investigate numerically the correlation between ground stiffness and η for two different distributions of trees. All calculations are performed in the MATLAB computational environment.

The ground of the forest environment is modelled as a discrete semi-infinite cubic lattice of masses with mass m, inter-mass spacing a, connected via springs of stiffness β_1. The cubic lattice is cleaved along its horizontal face (i.e., (001) plane), thus forming the surface of the ground; it is infinite in all other directions parallel to the plane. Therefore, the ground exhibits uniform composition throughout its depth and lacks irregular spatial variability. The top of permafrost can occur some depth below the surface of the ground, this non-permafrost layer, dubbed "overburden" can have a thickness on the order of metres (Wagner et al., 2018). However, permafrost itself can penetrate tens of metres or hundreds of metres into the ground. Seismic waves occur at wavelengths on the order of tens of metres to kilometres (Lay and Wallace, 1995), therefore the thickness of the overburden is both less than the thickness of the permafrost and on a sub-wavelength scale of seismic waves. Therefore, the ground can be approximated as homogenous permafrost along its depth.

Trees in the forest are theoretically modelled as discrete one-dimensional chains of masses with mass m and inter-mass spacing a, identical to the ground. The masses are connected via springs of stiffness β_2 and each tree is anchored to the cubic lattice of the ground via a spring of stiffness β_I. For simplicity $\beta_2 = \beta_I = 1$. Each tree contains only two masses and is identical to one another, and thus have identical vibrational resonances.

For simplicity, only displacements in one direction are considered in the equations used to model the elastic response of the system. The polarization of the acoustic wave is unspecified and can either be a transverse or longitudinal. The Interface Response Theory (IRT) (Dobrzynski, 1987, 1988) allows for the calculation of the diffusion matrix of the Green's function for the entire system composed of trees connected to ground surface. The diffusion matrix is used in calculating the scattered wave's phase with respect to frequency. Details on the calculation on the diffusion matrix and the Green's function can be found in Appendix A. The Green's function for the trees and the cubic lattice are calculated at runtime using MATLAB. The two-dimensional Fourier transform of the Green's function associated with the cubic lattice is calculated (See Eq. A.6), then converted from k-space to real space using MATLAB's native *ifft2* method. After the relationship between the geometric phase η and the frequency ω is calculated for a particular spatial distribution of trees, we ascertain the relationship between the geometric phase and the stiffness of the ground. We consider a forest environment to be composed of N_c mass-spring chains (trees) whose spatial distribution over the surface of the cubic lattice (ground) can described by the $2N_c$ dimensional vector M. M encodes the 2D coordinates of every tree. This vector contains the subset R of M, the set of the possible locations for trees to occupy, for the system defined in the Appendix A as (see Eq. (A.13)):

$$R = \left\{ p_1 = (0,0,0)\,, p_2 = \left(x_1^{'}, x_2^{'}, 0\right)\,, p_3 = (x^{'}{}_1, x^{'}{}_2, 0)\,, \ldots, p_{N_c} = \left(x_1^{(N_c-1)}\,, x_2^{(N_c-1)}\,, 0\right) \right\}$$

where $p_i = (x_1^{(i)}, x_2^{(i)}, 0)$ defines a 2D position on the (001) surface of the cubic lattice. The $x_I^{(i)}$ are integral multiples of the inter-mass spacing of the cubic lattice a. Following Appendix A, the phase difference between an acoustic wave carried by the coupled system (trees elastically coupled to the ground) and a wave carried by the uncoupled system (trees not coupled) is calculated from the relation: $\eta(R\epsilon M, \omega, \beta_1) = -\frac{1}{\pi} Im[ln(det\ \overleftrightarrow{\Delta}(MM))]$ where $\overleftrightarrow{\Delta}(MM)$ is the diffusion matrix. This matrix links the Green's function of the coupled system, $\overleftrightarrow{g}(MM)$, to the Green's function of the uncoupled system, $\overleftrightarrow{G}(MM)$. This coupling is achieved via the relation $\overleftrightarrow{g}(MM)\overleftrightarrow{\Delta}(MM) = \overleftrightarrow{G}(MM)$ in the space M. Since $ln(det\overleftrightarrow{\Delta}(MM)) = -ln(det\overleftrightarrow{g}(MM)) + ln\left(det\overleftrightarrow{G}(MM)\right)$, $\eta(R\epsilon M, \omega, \beta_1)$ represents the difference in phase between the coupled and uncoupled systems. We can now consider two possible values of ground stiffness, namely β_1 and $\beta_1{}'$. The quantity $\Delta\eta = \eta(R, \omega, \beta_1) - \eta(R, \omega, \beta_1{}')$ is the difference between the geometric phase of ground stiffness β_1 and $\beta_1{}'$ for a given tree distribution R. Since the trees in the uncoupled system are not connected to the ground, the phase of the uncoupled system remains the same regardless of tree distribution and therefore cancels out in the expression of $\Delta\eta$. As a result, the change in geometric phase can be calculated as the stiffness of the ground varies.

In this model the ground is taken as a homogenous ideal medium, however, the approach described here can also be applied to grounds containing heterogeneities which do not vary on the timescale of changes in the subsurface temperature of the permafrost. In our ideal system $\eta(R\epsilon M, \omega, \beta_1)$ represents the difference in phase between an ideal homogenous ground coupled with trees and the same system without the tree-ground coupling. The ideal nature of the ground of this model is found in the expression for $\overleftrightarrow{g}_{S1}$ in the appendix, however, for a non-ideal heterogenous ground, our model will differ from the ideal only in the functional form of $\overleftrightarrow{g}_{S1}$. We anticipate that this new function will still depend on the permafrost part of that heterogeneous ground. This means that as the permafrost below the active layer thaws it will still affect the functional form of $\overleftrightarrow{g}_{S1}$ similar to the case of the homogeneous ground. We will still be able to define the $\Delta\eta$, the difference in phase between the frozen and thawed ground/trees coupled system. $\Delta\eta$ is expected to be most sensitive near tree resonances. These resonances will occur at low frequencies, on the order of tens, to hundreds, of hertz (Colombi et al., 2016). At these low frequencies, the wavelength of the wave in the ground is on the order of hundreds of metres (Colombi et al.,

2016), therefore heterogeneities on a scale smaller than the wavelength will not interact with the wave and the ground can be taken to be an effective homogenous medium. Other factors that could affect the geometric phase such as moisture content or seasonal ice may occur on timescales different from permafrost thaw. Lighter vegetation may have minimal effect the geometric phase due to not having resonances in the frequency regime of interest.

Two forest environments with differing tree distributions were considered. In one distribution, 30 trees were placed in a semi-random manner far enough apart as to not interact with one another (Fig. 2 (b)) (see Appendix A for details on the cut-off distance of interaction of trees). In the other distribution, 30 trees were placed in a tight cluster (Fig. 2(c)). For each distribution the stiffness of the ground, β_1, was varied from 0.2 to 2.0. The masses, inter-mass spacing, and stiffness of the trees were kept constant $m = \beta_2 = \beta_I = a = 1$. The geometric phase was calculated for both types of distributions with different values of ground stiffness.

It has been observed in Yang et al., 2015, that the elastic modulus, a measure of ground stiffness, of permafrost varies inversely with temperature from as high as 8 GPa to as low as 2 GPa over a range of -12 °C to -1 °C, thus indicating a temperature dependent relationship of permafrost stiffness. In that study the field samples were collected and maintained at a uniform temperature during unconfined compression tests. For black spruce, a tree present within the boreal regions of Canada, the modulus of elasticity varies between 5 GPa and 17 GPa (Giroud et al., 2016). The elastic moduli of the ground and trees are proportional to the spring stiffnesses β_1 and β_2, respectively. Using the lower limit of elastic modulus for black spruce, the ratio of the ground's elastic modulus to that of the trees would vary over a range of 0.4 to 1.6. For temperatures above -1 °C it is assumed that the elastic modulus of the permafrost would continue to decrease, possibly allowing the ratio of elastic moduli to approach 0.2. Since the stiffness of the trees, $\beta_2 = 1$, in our model is held constant, the ratio of the stiffness of the ground relative to the trees is equal to β_1. Therefore, β_1 was varied over the range 0.2 to 2.0.

3. Results

The variation in density of states (see Eq. (A.12)) was calculated for the environment with the sparse distribution of trees (Fig. 2(b)) for both $\beta_1 = 0.2$ and $\beta_1 = 2.0$. The frequency ω is expressed in units reduced by the factor $\sqrt{\frac{\beta_2}{m}}$. Peaks in the figure correspond to the resonant frequencies of the trees. In Fig. 3(b) it is shown that for $\beta_1 = 0.2$ there is only one peak; this is because at $\beta_1 = 0.2$ the ground cannot support waves with a frequency above 0.859. The value of this frequency cut-off is determined by $\omega_{\text{cutoff}} = 2\sqrt{\frac{\beta_1}{m_1}}$. The varying stiffness of the ground changes the frequency regime available for propagating waves, with higher values of β_1 allowing waves of higher frequency. At $\beta_1 = 2.0$ the second resonance of the trees is observable (Fig. 3(b)). The two resonances arise from the trees being composed of only two masses. Because the trees are a sufficient distance apart as to not interact with one another through the ground, the resonances are degenerate.

In Fig. 3(b) it can be seen that the frequency at which the first resonance occurs changed with ground stiffness β_1. This phenomenon arises from the masses of the tree being coupled to a mass in the substrate, whose vibrational properties are subject to changes in the stiffness of the ground. This change in resonant frequency of trees with varying ground stiffness has been observed in numerical simulations of

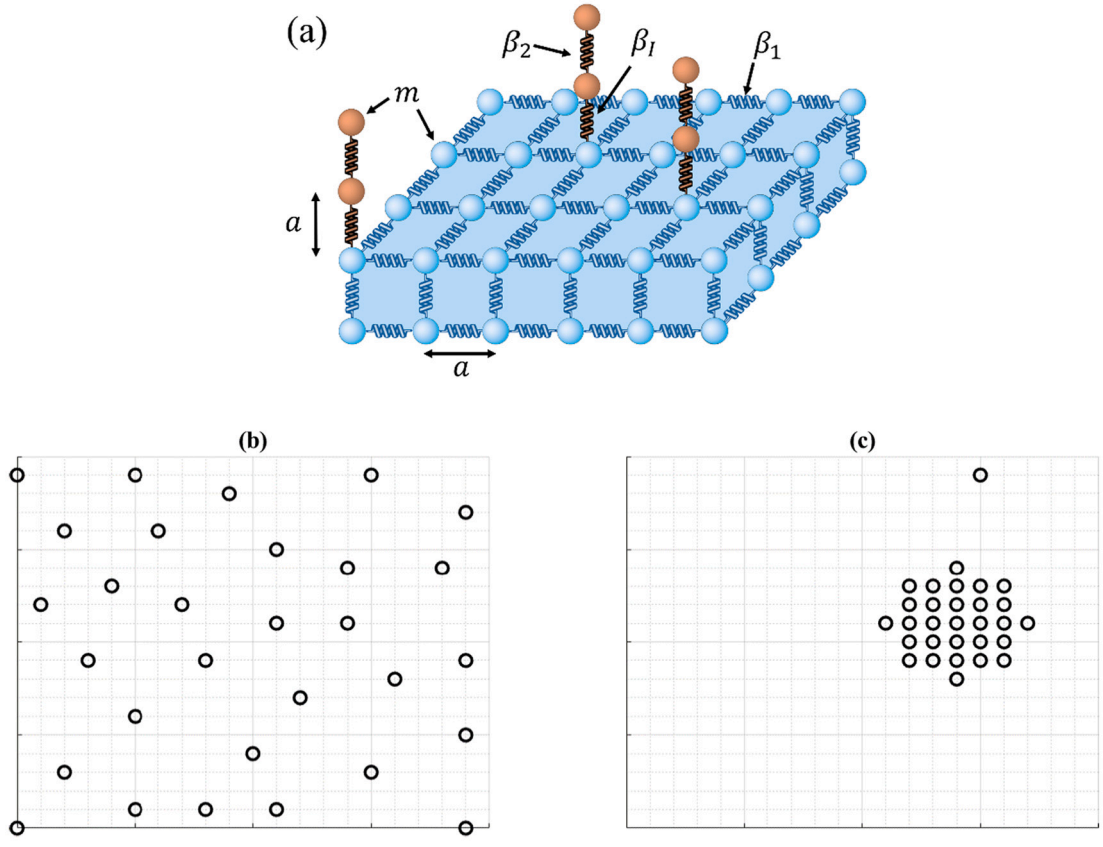

Fig. 2. (a) Ground-forest environment modelled as a lattice of masses (spheres) connected via springs. The system is composed of trees (orange) connected to the ground (light blue). The ground extends infinitely in directions that are not the surface. (b) A top-down view of the locations of trees for a sparse and random distribution. The trees occupy an area of $20a$ by $20a$. (c) A top-down view of the locations of trees in a dense cluster. The space (surface) spanned by the distribution of trees is denoted as R in this paper. (For interpretation of the references to colour in this figure legend, the reader is referred to the web version of this article.)

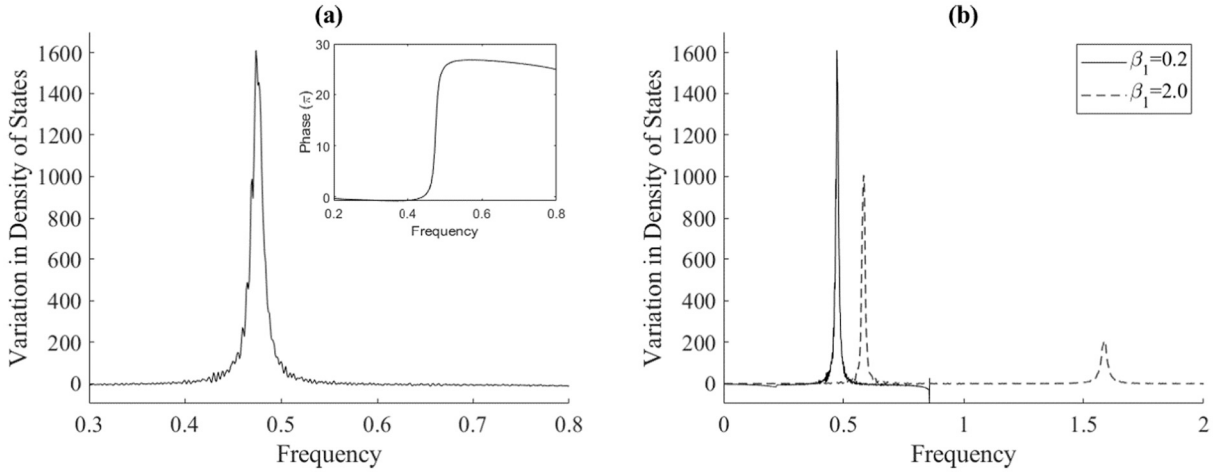

Fig. 3. (a) Variation in density of states for $\beta_1 = 0.2$. Inset is the geometric phase, $\eta(\omega)$, as a function of frequency showing that resonant frequencies correspond to sharp changes in the phase. (b) The calculated variation in density of states for a ground stiffness of $\beta_1 = 0.2$ and $\beta_1 = 2.0$. The first resonance occurs around a frequency of 0.474 for the lower β_1 value and around 0.585 for the higher β_1 value.

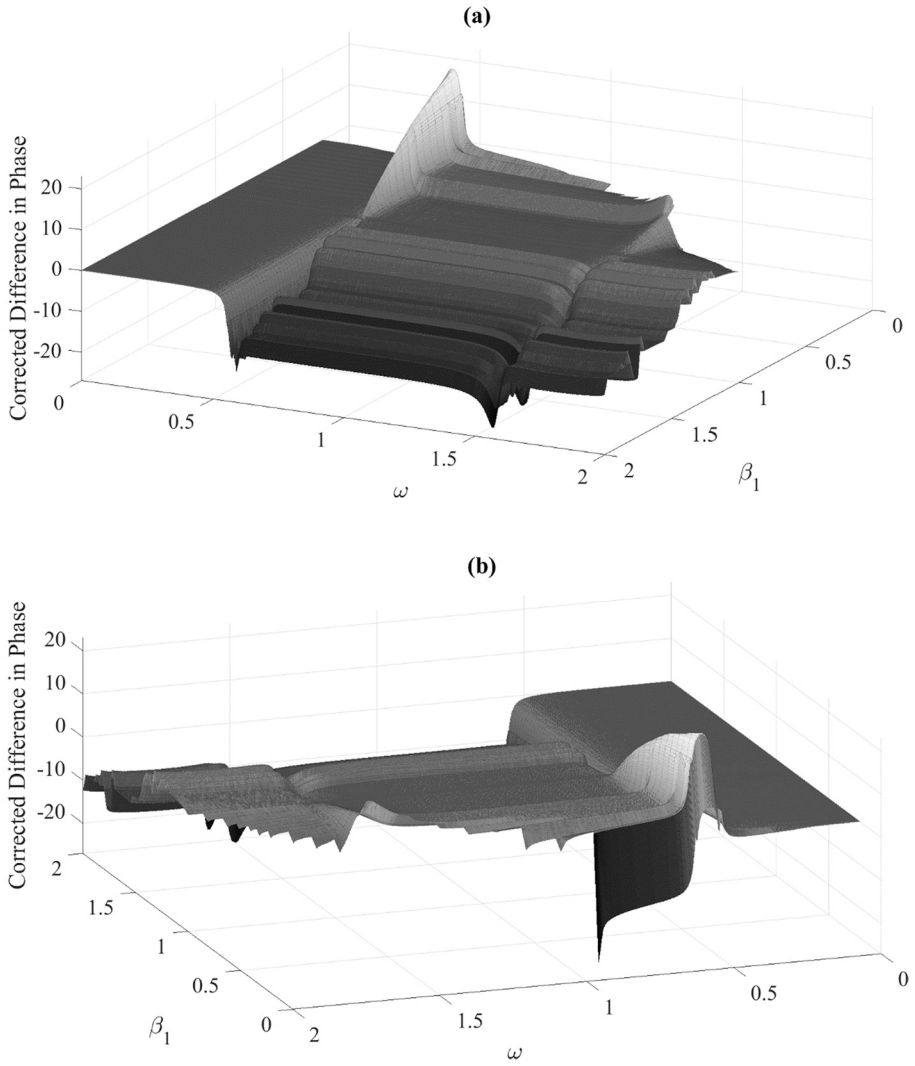

Fig. 4. (a) The corrected difference in phase for a distribution of sparse non-interacting trees (Fig. 2(b)) from $\beta_1 = 0.2$ to $\beta_1 = 2$ for select values of β_1. The frequency ω is reduced by the same factor $\sqrt{\frac{\beta_2}{m}}$. (b) Same plot as panel (a) but rotated to highlight the width of the peak around the first resonance and the cut-off phenomenon at lower values of β_1.

seismic wave propagation in forest environments (Colombi et al., 2016).

For each given distribution of trees, the phase $\eta(\omega,\beta_1)$ was calculated numerically. The case when the stiffness of the ground is equal to the stiffness of the trees, $\beta_1 = 1$, was selected as a reference β_1. The change in phase for a stiffness β_1' from the reference is expressed as $\Delta\eta = \eta(\omega,\beta_1') - \eta(\omega,\beta_1 = 1)$. Because phase is a periodic quantity with a period of 2π, e.g. $0 = 2\pi = 4\pi$, a phase difference $\Delta\eta$ that is an integer multiple of 2π is trivial and must be removed for clarity. For a given ground stiffness β_1', the phase difference at frequency ω_i, $\Delta\eta(\omega_i)$, had integral multiples of $\pm 2\pi$ added until for every frequency $|\Delta\eta(\omega_i,\beta_1') - \Delta\eta(\omega_{i-1},\beta_1')| < 2\pi$. This correction was done using in-house developed MATLAB code. A 3D plot of this corrected $\Delta\eta(\omega_i,\beta_1')$ for one of the distribution of trees was plotted in MATLAB and is shown in Fig. 4.

In Fig. 4 the troughs and hills along the β_1 axis in the surface occur near the resonant frequencies of the trees. Away from these frequencies it is observable that along the β_1 axis the difference in phase remains nearly zero; the curvature along the β_1 axis, particularly for values of $\beta_1 > 1$ arises from 2π jumps between different ground stiffnesses. These 2π jumps occur because the initial correction was done only along the frequency axis. From Fig. 4 it is clear that frequencies near the resonant frequencies of the trees will be of greater interest in measuring changes in ground stiffness. Calculation of the phase difference between a treeless frozen ground and an unfrozen ground would only lead to linear changes. The resonance associated with a tree's vibration is essential to achieve nonlinear changes in the phase difference between the frozen and unfrozen forested ground. A frequency of $\omega = 0.575$ near the first resonance, was selected and the difference in phase was calculated as a function of β_1 and corrected for 2π jumps. This calculation was performed for both the sparse and clustered distributions of trees and the results given in Fig. 5. A moving mean average was used to diminish minor discontinuities arising from the small fluctuations inherent in the numerical nature of the calculations. The local slope of the data was also plotted. The nonlinear variation in the difference in phase resulting from the interactions between tree resonances and changes in ground stiffness are discussed in the next section.

4. Discussion and conclusions

Detecting changes in arctic ground remains an active area of research concerning climate models and assessing risk to local resources and infrastructure. Here we show that changes in geometric phase resulting from variations in the effective stiffness of a forest floor can be used in theory to detect changes in ground properties, namely subsurface temperature. The nonlinear behaviour and sensitivity in the change of geometric phase with the state of the permafrost results from the interaction between the resonant vibrations of the trees and the ground. This method necessitates the trees, the trees' resonance enhances significantly the response of the phase difference to changes in the ground properties.. The workflow presented here provides an alternative to traditional aerial and satellite-based methods of remotely sensing permafrost thaw which suffer from operational costs or discontinuous monitoring.

Fig. 5(a) shows that the magnitude of the slope of the corrected difference in phase is greatest for the interval $1.05 < \beta_1 < 1.65$. In this regime, a given change in the stiffness of the ground produces a large change in the difference in corrected phase. This means that there is an enhanced ability to detect changes in permafrost stiffness due, e.g., to increasing subsurface temperature. Additionally, the slope has a minimum at $\beta_1 = 1.4$, which indicates an inflection point in the difference in phase. This can be used to distinguish between the stiffnesses above and below the inflection point. This behaviour is observed only for the distribution of sparse trees (Fig. 2(b)) which is representative of regions where the distance between trees typically is greater than the height of the trees themselves, like arctic taiga. A terrestrial-based remote sensing platform could be highly valuable in providing early warning of changing subsurface temperatures and permafrost thaw, which could result in damage by subsidence to infrastructure such as roads and railroads.

Fig. 5(b) shows that the profile of the change in phase is significantly different from that of the distribution of sparse trees, highlighting the importance of the knowledge of tree distribution in amplifying changes in phase. It can be observed that the slope of the difference in phase has a sign change around $\beta_1 = 1.025$. For this profile, the change in the sign of the slope can be exploited as a useful characteristic in clearly distinguishing between ground stiffness above and below this point. Additionally, the magnitude of the slope is quite large over a certain regime of β_1, making slight differences in ground stiffness, and thereby subsurface temperature, easier to detect. This distribution is representative of the more densely packed or clustered forests present in some regions of the arctic where there is little exposed ground for aerial and satellite-based observations.

The acoustic response of a system can be measured utilizing two different approaches. One way is to excite an acoustic wave at one place in the environment and measuring the response using a seismic detector at another location. The response recorded by the detector can then be used to relate changes in the seismic wave's geometric phase to changes in permafrost properties Another approach is to use two seismic

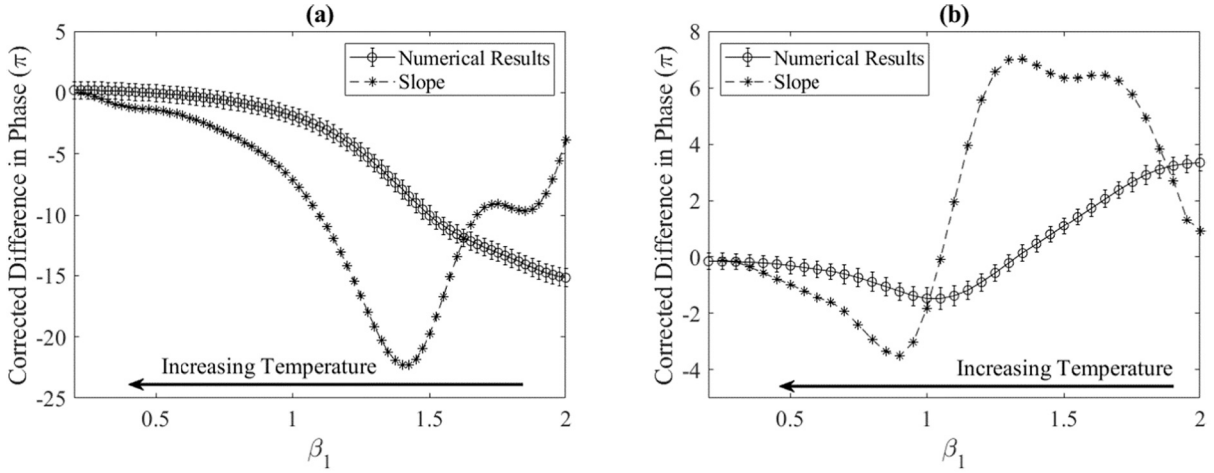

Fig. 5. (a) Numerically calculated corrected difference in phase for a configuration of non-interacting trees at a frequency of 0.575, and the local slope. (b) Numerical data for corrected difference in phase for a configuration of clustered trees at a frequency of 0.575 and its slope. In both panels, arrows indicate the direction β_1 evolves in with increasing temperature. Error bars are included to show that small variations in the slope may be artefacts of the numerical calculation.

detectors to measure acoustic waves latent in the environment arising from human and natural processes (Campillo, 2006; Derode et al., 2003; Sanchez-Sesma and Campillo, 2006). The spectra of the two sensors can be cross-correlate to extract the Green's function and its phase – this approach can be considered "passive" since it does not require exciting acoustic waves in the environment. This workflow can be enhanced via machine learning techniques and data mining which will allow for the extraction of signals from noisy data. In our model, an arbitrary area of $20a$ by $20a$ was selected for the numerical simulations; however, since the geometric phase is a global measure of the environment, the resolution of this method as a means of sensing can be adjusted by placing seismic sensors closer or farther apart as desired. Thus, GIS maps of permafrost distribution such as in Fig. 1 can be augmented with finer resolution data and continuous monitoring, especially in regions of continuous permafrost distribution below the overlaid treeline. Additionally, sensors can be placed to take advantage of specific tree distributions. This can allow for high resolution monitoring in areas of increased interest such as along existing infrastructure and around natural resources; and lower resolution monitoring in more remote regions. There is thus much flexibility in the operating costs of the acoustic method.

The sensitivity and applicability of this method depends largely on the distribution and characteristics of wave-scattering elements of the environment itself, such as trees in a forest. The wave-scattering elements do not need to be trees and can be any feature with resonances in the frequency regime of interest. These resonating features could be manmade to expand this remote sensing platform to regions without resonating features such as the Tibetan plateau. This leads to certain environments dramatically enhancing the effectiveness in detecting changes to permafrost. Previous work has explored the effect the distribution of wave-scattering elements such as trees have on the geometric phase, however, the combination of the two effects has yet to be fully explored. The model presented here does not account for heterogeneities in the ground composition such as the presence of massive rocks.

Future work will represent vertical variation in ground stiffness by utilizing a Green's function of a ground composed of a surface layer on top of a semi-infinite bulk. This surface layer can be used to investigate effects of season thaw and freezing of the permafrost active layer as well as detection depth. The approach could also be refined to address how other ground properties related to ground stiffness, such as organic or moisture content change in response to climate warming.

Author contributions

All authors contributed equally to the research and writing of the manuscript.

Declaration of Competing Interest

The authors declare that they have no known competing financial interests or personal relationships that could have appeared to influence the work reported in this paper.

Acknowledgements

This research did not receive any specific grant from funding agencies in the public, commercial, or not-for-profit sectors.

Appendix A

The system of interest can be broken down into a semi-infinite simple cubic lattice of masses and springs cleaved along the (001) surface and a finite 1-D chain coupled to the cubic lattice with a spring with stiffness β_I. The calculation of the Green's function of this system starts with the block matrix representing the Green's function where the chain is not coupled to the cubic lattice ($\beta_I = 0$):

$$\overleftrightarrow{G}_S = \begin{pmatrix} \overleftrightarrow{g}_{S1} & \overleftrightarrow{00} \\ \overleftrightarrow{00} & \overleftrightarrow{g}_{S2} \end{pmatrix}, \tag{A.1}$$

where $\overleftrightarrow{g}_{S1}$ and $\overleftrightarrow{g}_{S2}$ are the Green's functions of the lattice and the chain, respectively. These functions describe the elastic response of the lattice and chain for elastic waves of any polarization. To keep our model simple, we set the masses of the cubic lattice and chain to be the same, m, i.e., the densities of the trees and permafrost are comparable. The cubic lattice possesses a spring constant β_1 and the chain has a spring of β_2. The masses in the chain have a spacing a. For a finite harmonic chain with length L, the coordinates along the chain can be expressed as integral multiples of a such that $x = na$ for $n, n' \in [1, L]$. The Green's function is then (Deymier, 2013) given by

$$g_{S2}(n,n') = \frac{m}{\beta_2}\left[\frac{t^{|n-n'|+1} + t^{n+n'}}{t^2-1} + \frac{t^{2L+1}}{(t^2-1)(1-t^{2L})}\left(t^{n'-n} + t^{n-n'} + t^{1-n-n'} + t^{n+n'-1}\right)\right] \tag{A.2}$$

where

$$t = \begin{cases} \xi - \left(\xi^2 - 1\right)^{1/2} \text{ if } \xi > 1 \\ \xi + \left(\xi^2 - 1\right)^{1/2} \text{ if } \xi < -1 \\ \xi + i\left(1 - \xi^2\right)^{1/2} \text{ if } -1 \le \xi \le 1 \end{cases} \tag{A.3}$$

with

$$\xi = 1 - \frac{m\omega^2}{2\beta_2} \tag{A.4}$$

The frequency $\omega \in [0, \omega_0]$ with $\omega_0 = 2\sqrt{\frac{\beta_2}{m}}$. In this paper, a tree is a mass spring chain with $L = 2$.

The periodicity of Green's function of the cubic lattice allows it to be expressed as the inverse 2-D Fourier transform:

$$\overleftrightarrow{g}_{S1}(\omega, x_1, x_2, x_3) = \frac{1}{(2\pi)^2} \int_{-\frac{\pi}{a}}^{\frac{\pi}{a}} dk_1 \int_{-\frac{\pi}{a}}^{\frac{\pi}{a}} dk_2 e^{i(k_1 x_1 + k_2 x_2)} \overleftrightarrow{g}_{S1}(\omega, k_1, k_2, x_3) \tag{A.5}$$

Here, (x_1, x_2) are the coordinates on the cleaved (001) horizontal surface of the semi-infinite lattice. The surface is located at $x_3 = 0$. The spacing between masses in the cubic lattice is taken as a. The Green's function $\overleftrightarrow{g}_{S1}$ in k-space is given by (Akjouj et al., 1993)

$$\overleftrightarrow{g}_{S1}(\omega, k_1, k_2, x_3) = \frac{m}{\beta_1} \frac{t^{|n_3 - n_3'|+1} + t^{2-(n_3+n_3')}}{t^2 - 1} \tag{A.6}$$

with $n_3^{(\prime)} = \frac{x_3^{(\prime)}}{a}$.

The Green's function $g_{s1}(\omega, x_1, x_2, x_3 = 0)$ is calculated by substituting (A.6) into (A.5), where t is calculated using (A.7). From the dispersion relation of a simple cubic harmonic lattice: $\omega^2 = \frac{2\beta_1}{m}(3 - cosk_1 a - cosk_2 a - cosk_2 a)$ we can define.

$\xi = 3 - cosk_1 a - cosk_2 a - \frac{m\omega^2}{2\beta_1}$ (A.7).

Let a position on the surface of the cubic lattice be: $p_i = (x_1^{(i)}, x_2^{(i)}, 0)$, then we only calculate for every frequency $\omega \leq \omega_0$: $g_{S1}(p_i p_j) = g_{S1}(p_i - p_j = (x_1^{(j)} - x_1^{(i)}, x_2^{(j)} - x_2^{(i)}, 0))$ for $(x_1^{(j)} - x_1^{(i)}, x_2^{(j)} - x_2^{(i)}, 0) = \{(0,0,0), (0,1a,0), (0,2a,0), (1a,0,0), (2a,0,0), (1a,1a,0), (1a,2a,0), (2a,1a,0)\}$. We neglect all other g_{s1} in this paper. This means we consider an interaction between chains with a separation distance of $\left|p_i - p_j\right| = \sqrt{5}a$ for the Green's function $g_{S1}(p_i p_j)$.

Using IRT, a coupling operator is defined to couple the first mass (site 1) of mass-spring chain (base of a tree) to an arbitrary site $X = (x_1, x_2, x_3 = 0)$ on the cubic lattice:

$$\overleftrightarrow{V}_I = \begin{pmatrix} V_I(X,X) & V_I(X,1) \\ V_I(1,X) & V_I(1,1) \end{pmatrix} = \begin{pmatrix} \frac{-\beta_I}{m} & \frac{\beta_I}{m} \\ \frac{\beta_I}{m} & \frac{-\beta_I}{m} \end{pmatrix}. \tag{A.8}$$

For simplicity we set $\beta_I = \beta_2$. Using IRT we can define a surface operator over the space of coupled interface locations, M:

$$\overleftrightarrow{A}_0(MM) = \begin{pmatrix} A(X,X) \\ A(X,1) \\ A(1,X) \\ A(1,1) \end{pmatrix} = \begin{pmatrix} V_I(X,X) g_{S1}(X,X) \\ V_I(X,1) g_{S2}(1,1) \\ V_I(1,X) g_{S1}(1,X) \\ V_I(1,1) g_{S2}(1,1) \end{pmatrix}. \tag{A.9}$$

The diffusion matrix is written as a 2×2 matrix in the space, M, of the interface sites:

$$\overleftrightarrow{\Delta}(MM) = \begin{pmatrix} 1 + A(X,X) & A(X,1) \\ A(1,X) & 1 + A(1,1) \end{pmatrix} = \begin{pmatrix} 1 + V_I(X,X) g_{S1}(X,X) & V_I(X,1) g_{S2}(1,1) \\ V_I(1,X) g_{S1}(1,X) & 1 + V_I(1,1) g_{S2}(1,1) \end{pmatrix} \tag{A.10}$$

The phase difference between elastic modes in the coupled (trees anchored) and uncoupled (trees not anchored) systems in the space M, normalized to π, is given by:

$$\eta(\omega) = -\frac{1}{\pi} Im[ln(det\, \overleftrightarrow{\Delta}(MM))] \tag{A.11}$$

This represents the phase accumulated by an acoustic wave resulting from its scattering by the mass spring chains due to them being elastically coupled to the lattice. The variation in density of states arising from the coupling is then determined through:

$$\Delta n(\omega) = \frac{d\eta(\omega)}{d(\omega^2)} \tag{A.12}$$

Δn is the variation of the vibrational density of states between the trees anchored to the ground and the reference system composed of the cubic lattice with uncoupled trees.

Hitherto we have described a system with only one chain coupled the surface of the cubic lattice; this process can be generalized to N_c chains coupled to several sites on the cubic lattice The space M is now defined as

$$M = \left\{ p_1 = (0,0,0), 1, p_2 = \left(x_1', x_2', 0\right), 1', p_3 = (x'_1, x'_2, 0), 1'', \ldots, p_{N_c} = \left(x_1^{(N_c-1)}, x_2^{(N_c-1)}, 0\right), 1^{(N_c-1)} \right\} \tag{A.13}$$

The first finite mass-spring chain is situated at the origin on the lattice surface. Thus, the coupling operator is a $2N_c \times 2N_c$ matrix:

$$\overleftrightarrow{V}_I = \frac{\beta_I}{m} \begin{pmatrix} -1 & 1 & 0 & 0 & \ldots & 0 & 0 \\ 1 & -1 & 0 & 0 & \ldots & 0 & 0 \\ 0 & 0 & -1 & 1 & \ldots & 0 & 0 \\ 0 & 0 & 1 & -1 & \ldots & 0 & 0 \\ \vdots & \vdots & \vdots & \vdots & \ldots & \vdots & \vdots \\ 0 & 0 & 0 & 0 & 0 & -1 & 1 \\ 0 & 0 & 0 & 0 & 0 & 1 & -1 \end{pmatrix}. \tag{A.14}$$

To calculate the diffusion matrix, $\overleftrightarrow{\Delta}(MM) = \overleftrightarrow{I}(MM) + \overleftrightarrow{V}_I(MM)\overleftrightarrow{G}_S(MM)$, the Green's function of the uncoupled system, $\overleftrightarrow{G}_S(MM)$, is needed:

$$\overleftrightarrow{G}_s(MM) = \begin{pmatrix} g_{S1}(p_1p_1) & 0 & g_{S1}(p_1p_2) & 0 & g_{S1}(p_1p_3) & 0 & \dots & g_{S1}(p_1p_{N_c}) & 0 \\ 0 & g_{S2}(11) & 0 & 0 & 0 & 0 & \dots & 0 & 0 \\ g_{S1}(p_2p_1) & 0 & g_{S1}(p_2p_2) & 0 & g_{S1}(p_2p_3) & 0 & \dots & g_{S1}(p_2p_{N_c}) & 0 \\ 0 & 0 & 0 & g_{S2}(1'1') & 0 & 0 & \dots & 0 & 0 \\ g_{S1}(p_3p_1) & 0 & g_{S1}(p_3p_2) & 0 & g_{S1}(p_3p_3) & 0 & \dots & g_{S1}(p_3p_{N_c}) & 0 \\ 0 & 0 & 0 & 0 & 0 & g_{S2}(1^{(2)}1^{(2)}) & \dots & 0 & 0 \\ \vdots & \vdots & \vdots & \vdots & \vdots & \vdots & \vdots & \vdots & \vdots \\ g_{S1}(p_{N_c}p_1) & 0 & g_{S1}(p_{N_c}p_2) & 0 & g_{S1}(p_{N_c}p_3) & 0 & \dots & g_{S1}(p_{N_c}p_{N_c}) & 0 \\ 0 & 0 & 0 & 0 & 0 & 0 & \dots & 0 & g_{S2}(1^{(N_c-1)}1^{(N_c-1)}) \end{pmatrix}$$

(A.15)

In (A.15) the odd rows and columns correspond to sites on the lattice and even rows and columns correspond to the position of the fist mass in the 1D chains.

The diffusion matrix in the space M is

$$\overleftrightarrow{\Delta}(MM) = \overleftrightarrow{I} + \overleftrightarrow{A}(M,M) = \overleftrightarrow{I} + \overleftrightarrow{V}_I \overleftrightarrow{G}_s(MM). \tag{A.16}$$

The phase difference is again given by eq. (A.11).

References

Ajo-Franklin, J., Dou, S., Lindsey, N., Daley, T.M., Freifeld, B., Martin, E.R., Robertson, M., Ulrich, C., Wood, T., Eckblaw, I., Wagner, A., 2017. In: Timelapse Surface Wave Monitoring of Permafrost Thaw using Distributed Acoustic Sensing and a Permanent Automated Seismic Source. SEG International Exposition and 87th Annual Meeting, pp. 5223–5227. https://doi.org/10.1190/segam2017-17774027.1.

Akjouj, A., Sylla, B., Dobrzynski, L., 1993. Introduction to a theory of composite systems - simple examples of lamellar materials. Ann. Phys. Fr. 18, 363–448.

Berry, M.V., 1984. Quantal phase factors accompanying adiabatic changes. Proc. Royal Soc. A. 45–47.

Brown, J., Ferrians, O., Heginbottom, J.A., Melnikov, E., 2002. Circum-Arctic Map of Permafrost and Ground-Ice Conditions, Version 2 [WWW Document]. NSIDC Natl. Snow Ice Data Cent, Boulder, Color, USA.

Campillo, M., 2006. Phase and correlation in "Random" seismic fields and the reconstruction of the green's function. Pure Appl. Geophys. 163.

Colombi, A., Roux, P., Guenneau, S., Gueguen, P., Craster, R.V., 2016. Forests as a natural seismic metamaterial: rayleigh wave bandgaps induced by local resonances. Sci. Rep. 6, 1–7. https://doi.org/10.1038/srep19238.

De, C., Chakraborty, B., 2011. Model-based acoustic remote sensing of seafloor characteristics. IEEE Trans. Geosci. Remote Sens. 49, 3868–3877. https://doi.org/10.1109/TGRS.2011.2139218.

Derode, A., Larose, E., Campillo, M., Fink, M., 2003. How to estimate th Green's function of a heterogenous medium between two passive sensors? Application to acoustic waves. Appl. Phys. Lett. 83.

Deymier, P.A., 2013. Acoustic Metamaterials and Phononic Crystals. Springer, Berlin, Heidelberg. https://doi.org/10.1007/978-3-642-31232-8.

Deymier, P.A., Runge, K., 2017. Sound Topology, Duality, Coherence and Wave-Mixing An Introduction to the Emerging New Science of Sound. Springer Series in Solid State Sciences.

Dobrzynski, L., 1987. Interface response theory of discrete superlattices. Prog. Surf. Sci. 26.

Dobrzynski, L., 1988. Interface response theory of composite systems. Surf. Sci. 200.

Döpper, V., Panda, S., Waigl, C., Braun, M., Feilhauer, H., 2021. Using floristic gradient mapping to assess seasonal thaw depth in interior Alaska. Appl. Veg. Sci. 24, e12561.

Ford, J.D., Bell, T., St-Hilaire-Gravel, D., 2010. Vulnerability of Community Infrastructure to Climate Change in Nunavut: A Case Study from Arctic Bay, in: Community Adaptation and Vulnerability in Arctic Regions. Springer, Dordrecht.

Giroud, G., Bégin, J., Defo, M., Ung, C.H., 2016. Ecogeographic variation in black spruce wood properties across Quebec's boreal forest. For. Ecol. Manag. 378, 131–143. https://doi.org/10.1016/j.foreco.2016.07.031.

Hatlelid, W.G., MacDonal, J.R., 1982. Permafrost determination by seismic velocity analyses. J. Can. Soc. Explor. Geophys. 18, 14–22.

Hjort, J., Karjalainen, O., Aalto, J., Westermann, S., Romanovsky, V.E., Nelson, F.E., Etzelmüller, B., Luoto, M., 2018. Degrading permafrost puts Arctic infrastructure at risk by mid-century. Nat. Commun. 9 https://doi.org/10.1038/s41467-018-07557-4.

James, S.R., Knox, H.A., Abbott, R.E., Panning, M.P., Screaton, E.J., 2019. Insights into permafrost and seasonal active-layer dynamics from ambient seismic noise monitoring. J. Geophys. Res. Earth Surf. 124, 1798–1816. https://doi.org/10.1029/2019JF005051.

Kanevskiy, M., Liljedahl, A.K., Nolan, M., Walker, D.A., Jorgenson, M.T., Raynolds, M.K., Sturm, M., 2019. Likely Impacts of Proposed 3D-Seismic Surveys to the Terrain, Permafrost, Hydrology, and Vegetation in the 1002 Area, Arctic National Wildlife Refuge, Alaska. Alaska Geobotany Center, Fairbanks, Alaska.

Kneisel, C., Hauck, C., Fortier, R., Moorman, B., 2008. Advances in geophysical methods for permafrost investigation. Permaf. Periglc. Process. 19, 157–178. https://doi.org/10.1002/ppp.616.

Lata, T.D., Deymier, P.A., Runge, K., Le Tourneau, F.-M., Ferrière, R., Huettmann, F., 2020. Topological acoustic sensing of spatial patterns of trees in a model forest landscape. Ecol. Model. 419 https://doi.org/10.1016/j.ecolmodel.2020.108964.

Lay, T.C., Wallace, T., 1995. Modern Global Seismology. Academic Press, San Diego.

Linke, J., Franklin, S.E., Huettmann, F., Stenhouse, G.B., 2005. Seismic cutlines, changing landscape metrics and grizzly bear landscape use in Alberta. Landsc. Ecol. 20, 811–826. https://doi.org/10.1007/s10980-005-0066-4.

Mullet, T.C., Gage, S.H., Morton, J.M., Huettmann, F., 2016. Temporal and spatial variation of a winter soundscape in south-central Alaska. Landsc. Ecol. 31.

National Research Council, 2014. Opportunities to Use Remote Sensing in Understanding Permafrost and Related Ecological Characteristics: Report of a Workshop. Washington, DC. https://doi.org/10.17226/18711.

Nitze, I., Grosse, G., Jones, B.M., Romanovsky, V.E., Boike, J., 2018. Remote Sensing Quantifies Widespread Abundance of Permafrost Region Disturbances across the Arctic and Subarctic, Nature Communications. Springer US. https://doi.org/10.1038/s41467-018-07663-3.

Sanchez-Sesma, F.J., Campillo, M., 2006. Retrieval of the Green's function from cross correlation: The canonical elastic problem. Bull. Seismol. Soc. Am. 96.

Schuur, E.A.G., McGuire, A.D., Schädel, C., Grosse, G., Harden, J.W., Hayes, D.J., Hugelius, G., Koven, C.D., Kuhry, P., Lawrence, D.M., Natali, S.M., Olefeldt, D., Romanovsky, V.E., Schaefer, K., Turetsky, M.R., Treat, C.C., Vonk, J.E., 2015. Climate change and the permafrost carbon feedback. Nature 520, 171–179. https://doi.org/10.1038/nature14338.

Trapeznikov, V., Maleev, D., 2019. Seismic profile solution under conditions of thawing permafrost with technogenic depression. In: MATEC Web of Conferences 265, p. 04011. https://doi.org/10.1051/matecconf/201926504011.

Turk, A.S., Hocaoglu, K.A., Vertiy, A.A., 2011. Acoustic and seismic sensors. In: Subsurface Sensing. John Wiley & Sons, Incorporated, pp. 387–411.

Wagner, A.M., Lindsey, N.J., Dou, S., Gelvin, A., Saari, S., Williams, C., Ekblaw, I., Ulrich, C., Borglin, S., Morales, A., Ajo-Franklin, J., 2018. Permafrost degradation and subsidence observations during a controlled warming experiment. Sci. Rep. 8, 1–9. https://doi.org/10.1038/s41598-018-29292-y.

Yang, Z.J., Still, B., Ge, X., 2015. Mechanical properties of seasonally frozen and permafrost soils at high strain rate. Cold Reg. Sci. Technol. 113, 12–19. https://doi.org/10.1016/j.coldregions.2015.02.008.

Zhang, X., Xiao, M., Cheng, Y., Lu, M.H., Christensen, J., 2018. Topological sound. Commun. Phys. https://doi.org/10.1038/s42005-018-0094-4.